JOM, Vol. 72, No. 7, 2020
https://doi.org/10.1007/s11837-020-04169-6

Dry Metal Forming Using Volatile Lubricants Injected into the Forming Tool Through Flow-Optimized, Laser-Drilled Microholes

MANUEL HENN,[1,3] GERD REICHARDT,[2] RUDOLF WEBER,[1] THOMAS GRAF,[1] and MATHIAS LIEWALD[2]

1.—Institut für Strahlwerkzeuge, University of Stuttgart, Pfaffenwaldring 43, 70569 Stuttgart, Germany. 2.—Institute for Metal Forming Technology, University of Stuttgart, Holzgartenstrasse 17, 70174 Stuttgart, Germany. 3.—e-mail: manuel.henn@ifsw.uni-stuttgart.de

A novel tribologic system was developed in which volatile lubricants (carbon dioxide—CO_2 or nitrogen—N_2) were used as a substitute for mineral oil-based lubricants in deep drawing processes. This process allows an intermediate medium to be introduced into the tool contact surfaces under high pressure by flow-optimized, laser-drilled microholes. This eliminates the need for subsequent cost-intensive cleaning processes as volatile lubricants evaporate while expanding to ambient pressure without leaving any residue. This article gives an overview of the current findings to enable and characterize the novel tribologic system. The areas of microhole laser drilling by ultrashort pulsed laser radiation, characterization of the novel tribologic system and realization of the system using a prototype tool will be described.

INTRODUCTION

Mineral oil or wax-based lubricants are commonly used in deep drawing processes. To prepare the formed parts for subsequent process steps, time-consuming and cost-intensive cleaning steps are required, where the lubricants used may also contain toxic additives that pollute the environment.[1]

To avoid these problems, a novel tribologic system for deep drawing processes has been developed, which offers a substitute to the use of traditional lubricants.[2] Figure 1a shows a sketch of the operating principle of the novel tribologic system. During deep drawing of the sheet metal parts, liquid CO_2 or gaseous N_2 is fed into the friction zone between the forming tool and the sheet metal under high pressure by diffuser-shaped, laser-drilled microholes. Both media serve as volatile lubricants and evaporate free of residues after the drawing process.

To provide the necessary mechanical strength of the forming tools, a minimum wall thickness of 5 mm of hardened steel is required; therefore, the drilling depth for the microholes providing the volatile lubricant must be 5 mm as well. The required microhole geometry was determined with numerical simulation of the flow behavior within the microholes with the emphasis on a possible partial phase change from liquid to solid CO_2. A diffuser-shaped geometry with a gas inlet radius of $r_1 = 100\ \mu$m and an outlet radius of $r_2 = 300\ \mu$m met the requirements.[3] A schematic of this geometry is shown in Fig. 1b.

This article summarizes the results of friction experiments for the characterization of the new tribologic system and the process requirements for percussion laser drilling of the deep, longitudinally shaped microholes in hardened tool steel.

LASER DRILLING OF SHAPED MICROHOLES INTO THE FORMING TOOLS

Required Laser Pulse Energy and Pulse Repetition Rate

To produce microholes with a depth of several millimeters, a laser pulse energy of multiple millijoules is required. For the ablation-dominant percussion drilling process, Förster et al.[4] published an analytical model that allows the prediction of the maximum possible drilling depth and aspect ratio for a given spot diameter and pulse energy. A homogeneous distribution of the fluence, i.e. the

(Published online April 21, 2020)

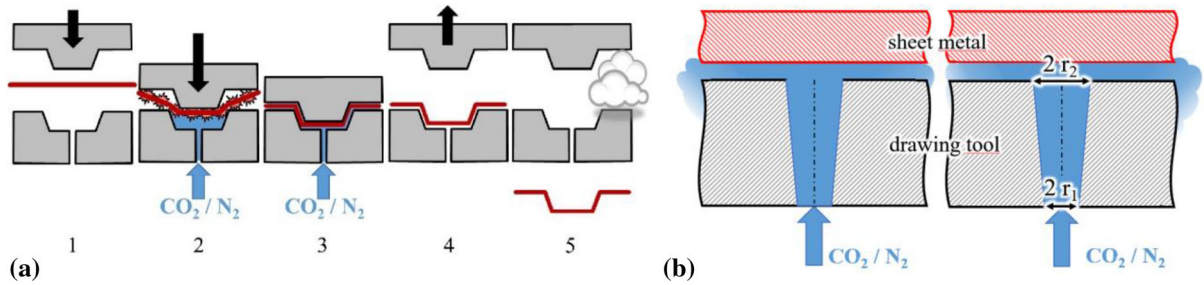

Fig. 1. (a) Operating principle of the drawing process using volatile lubricants. Adapted from Ref. 5. (b) Geometry of the required microholes in the forming tool.

laser pulse energy per unit area, on the inner surface of the cone-shaped microholes was assumed in this model. When this fluence reaches threshold fluence for ablation of the sample material, the drilling progress becomes significantly decelerated and discontinuous. This limit was also referred to as the "quality depth limit".[5]

Based on this model, the pulse energy E_p for a desired ablation radius r_{abl} and a given drilling depth z_{depth} can be written as

$$E_p = \phi_{th} \cdot \pi \cdot r_{abl} \cdot \sqrt{r_{abl}^2 + z_{depth}^2} \tag{1}$$

The size of the ablation radius as a function of the laser beam parameters will be discussed in "Microhole Radius on the Side of the Laser Impact" section. To create a conical microhole with a required ablation radius of r_2 = 300 μm and the required drilling depth of 5 mm, the necessary pulse energy amounts to approximately 4.4 mJ. For this example, a threshold fluence for steel of ϕ_{th} = 0.09 J/cm^2, at a wavelength of 800 nm and a pulse duration of 1 ps, was chosen.

Thermal damage due to heat accumulation is particularly critical when drilling in hardened tool steel. Heat accumulation can occur especially during laser-drilling with high average laser power and at high repetition rates.[6,7] To avoid heat accumulation, pulse repetition rates $<$ 50 kHz must be used[5] at pulse energies of a few millijoules.

Longitudinal Microhole Shaping

Microhole Radius on the Side of the Laser Impact

The radius of the microhole on the side of the laser impact is determined by the ablation radius. The ablation radius is determined by the ablation threshold, i.e. where the local fluence in the Gaussian beam is equal to the ablation threshold. The Gaussian function for the fluence at the position z in the direction of beam propagation is given by

$$\phi(r,z) = \phi_0(z) \cdot exp\left(-\frac{2 \cdot r^2}{r_{beam}(z)^2}\right), \tag{2}$$

where the peak fluence of a Gaussian beam is defined by

$$\phi_0(z) = \frac{2 \cdot E_p}{\pi \cdot r_{beam}(z)^2}. \tag{3}$$

The beam radius $r_{beam}(z)$ as a function of the position along the propagation in z direction is given by

$$r_{beam}(z) = w_0 \cdot \sqrt{1 + z^2 \cdot \left(\frac{M^2 \cdot \lambda}{\pi \cdot w_0^2}\right)^2}, \tag{4}$$

where w_0 is the radius of the beam in the focus, M^2 the beam quality and λ the wavelength of the laser beam. The Gaussian function for the fluence is plotted as a solid line in Fig. 2a for the example of a pulse energy of 5 mJ. At a fluence of ϕ_0/e^2, the beam radius r_{beam} is marked with a dashed red line. The ablation radius where $\phi = \phi_{th}$ is marked with a dotted green line.

The pulse energy E_p and distance z in beam propagation are used in the following to set the ablation radius. With the necessary fluence for ablation $\phi(r,z) = \phi_{th}$, the ablation radius at the position z for a given pulse energy can be derived from Eq. 2, and is given by

$$r_{abl}(z,E_p) = r_{beam}(z) \cdot \sqrt{\frac{1}{2} ln\left(\frac{2 \cdot E_p}{\pi \cdot r_{beam}(z)^2 \cdot \phi_{th}}\right)}. \tag{5}$$

Figure 2b shows the beam radius $r_{beam}(z)$ along the propagation direction z (the ordinate) for a focal length of 600 mm and a raw beam diameter on the focussing lens of 10 mm as a dotted red line. In addition, the ablation radius $r_{abl}(z)$ is plotted for the pulse energy of E_p = 0.5 mJ (blue line) and for E_p = 5 mJ (green line). The ablation radii near the focal point, at z = 0, are similar for both pulse

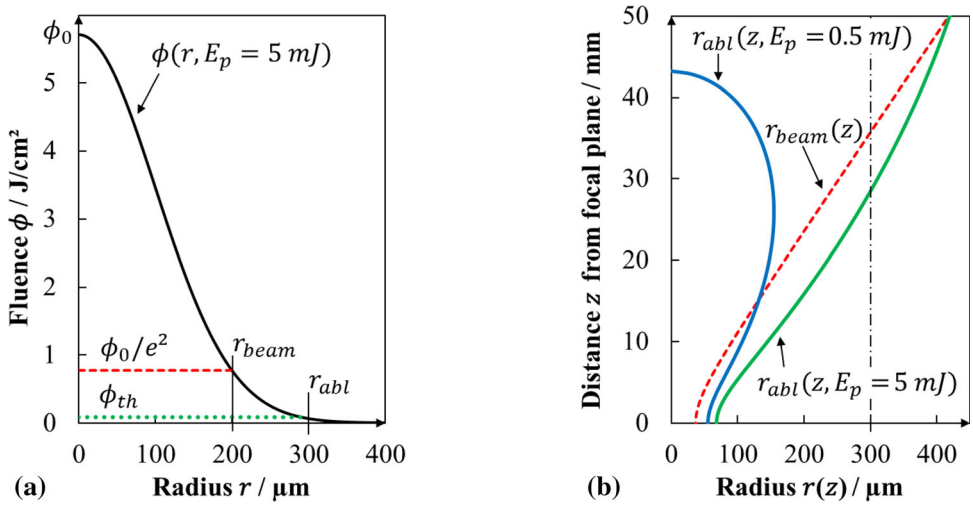

Fig. 2. (a) Fluence as a function of r for a Gaussian laser beam with a pulse energy of 5 mJ. Peak fluence is given as ϕ_0. The beam radius r_{beam} is at the fluence of ϕ_0/e^2 (dashed red line). The ablation radius r_{abl} is achieved when $\phi(r, E_p) = \phi_{th}$ (dotted green line). (b) Shows the beam radius $r_{beam}(z)$ along the propagation direction z (ordinate) as a dashed red line. In addition the ablation radius $r_{abl}(z)$ is plotted for the pulse energy of E_p = 0.5 mJ (blue line) and for E_p = 5 mJ (green line) (Color figure online).

Table I. Process parameters used for the experiments

Laser system: spectra physics spitfire *H*		
Wavelength	λ	800 nm
Beam quality	M^2	< 1.2
Max. pulse energy	E_p	7 mJ
Pulse repetition rate	f_{rep}	1 kHz
Max. average power	P	7 W
Pulse duration	τ	1 ps
Raw beam diameter	D_r	10 mm
Focal length	f_L	600 mm
Focal radius	w_0	37 μm
Rayleigh-length	z_R	4.400 mm

energies. However, this changes for increasing z. In the case of a pulse energy of 0.5 mJ, ablation is only possible for $z < 45$ mm. Furthermore, the pulse energy of 0.5 mJ is not sufficient to produce an ablation radius of 300 μm (marked with the vertical dash-dotted black line). In comparison, an ablation radius of about 400 μm is achieved at z = 45 mm with a pulse energy of 5 mJ, whereas the ablation radius of 300 μm is achieved at $z \approx 27$ mm.

With the given pulse energy and ablation threshold, the possible ablation radius for any position in z of the sample surface can be precisely determined using the analytical model shown in this chapter.

DRILLING OF THE SHAPED MICROHOLES

Experimental Setup for Percussion Drilling

A Ti:sapphire laser was used for the experiments. The specifications of the laser beam source are listed in Table I. The low repetition rate of 1 kHz ensured

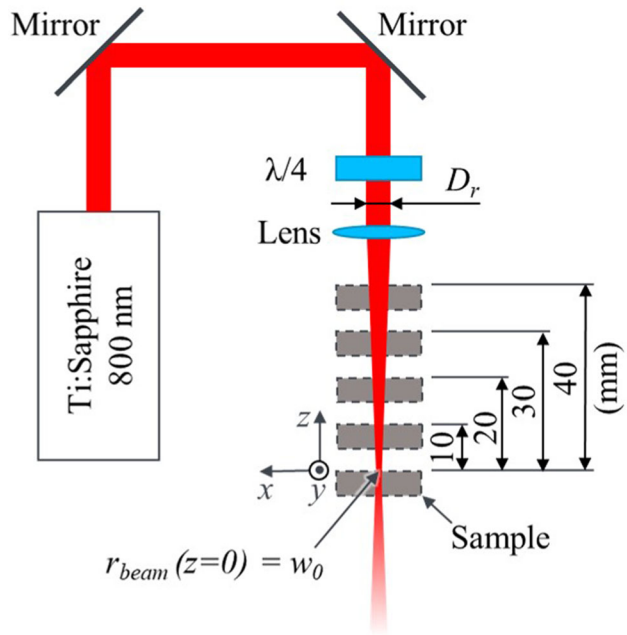

Fig. 3. Experimental setup for laser drilling. The linearly polarized raw laser beam with a beam diameter of D_r = 10 mm was circularly polarized with a $\lambda/4$ wave plate, and focused with a quartz focusing lens with a focal length of f = 600 mm onto the samples, which were mounted on a xyz-translation stages. The z-axis was used to set the distance of the sample in the beam propagation direction relative to the focal plane (represented by dashed gray rectangles) allowing to set the spot size on the sample surface.

that heat accumulation is avoided as described above. The experimental setup is sketched in Fig. 3. The linearly polarized raw laser beam was circularly polarized passing through a $\lambda/4$ wave plate, and focused with a quartz focusing lens with a focal length of f = 600 mm onto the samples, which were mounted on xyz-translation stages. The two

axes x and y were used for repositioning the sample for the individual microholes. The z-axis was used to set the distance of the sample in the beam propagation direction relative to the focal plane (represented by dashed gray rectangles) allowing to set the spot size on the sample surface. With the raw beam diameter of D_r = 10 mm, the calculated focus radius was approximately $r_{beam}(z = 0) = w_0 = 37$ μm. Due to the good availability, stainless steel (1.4301) was used as sample material.

Figure 4 shows the measured ablation radii of the drilled microholes for z = 0 mm, 10 mm, 20 mm, 30 mm and 40 mm, indicated as blue triangles. The data points are connected with a dotted line to guide the eye. The calculated ablation radius for a given pulse energy of 5 mJ according to Eq. 3 is shown as a solid green line. For this example, the fluence threshold was set to 0.05 J/cm^2 to fit to the measured values. The measured ablation radius differs from the calculated for $z \leq 10$ mm. Laser pulses with short pulse duration and high pulse energy can cause an air breakdown, particularly in the vicinity of the focus, if $> 10^{13}$ W/cm^2 is achieved.[8,9] The ionization of the air causes a change of the refractive index resulting in a strong defocusing of the incident laser beam. This results in an increased spot size on the sample surface and therefore a change of the ablation radius compared with the calculated r_{abl}. This effect is particularly pronounced when the pulse duration is reduced to the femtosecond range.[9] The quality of the microhole can be significantly improved by avoiding this effect.

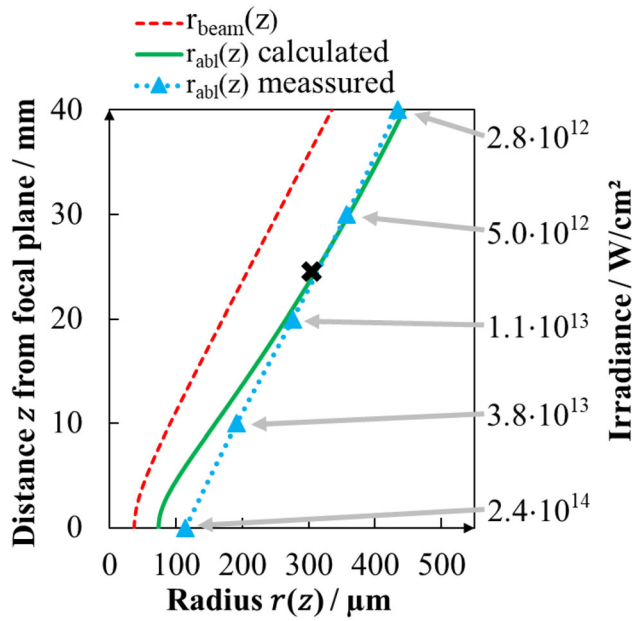

Fig. 4. Calculated (green line) and measured (blue triangles) ablation radii (r_{abl}) plotted for increasing z. The data points are connected with a dotted line to guide the eye; the pulse energy was 5 mJ. In addition, the beam radius $r_{beam}(z)$ is drawn as a dashed red line. For this example, the fluence threshold was set to 0.05 J/cm^2 to fit the measured values (Color figure online).

Drilling of Microholes in the Forming Tools

For the production of the microholes into the forming tools made of hardened tool steel (1.2379), the same setup as described in the previous section was used. The two steels 1.4301 and 1.2379 showed very similar results with the same drilling parameters. To meet the gas-outlet radius of r_2 = 300 μm with the ablation radius, a distance of approximately z = 25 mm of the sample surface from the focus position was necessary (marked with a cross in Fig. 4). Figure 5 shows a cross-section of a microhole. The sample was etched with an Adler solution for 30 s. The effect of heat accumulation was successfully avoided as no heat-affected zone is apparent. Apart from a slight transverse bulge in the upper half, the general shape of the microhole is mostly conical and therefore very similar to the ideal shape. In addition, the gas-outlet (top) and gas-inlet (bottom) cross-sections are shown on the right-hand side. The dotted circles represent equivalent cross-sectional areas where the radius was approximately r_2 = 300 μm and r_1 = 50 μm, respectively. The shape of the hole on the important gas-outlet side is very close to the required circle. On the gas-inlet side, the cross section is rather rectangular than circular. However, the shape on the inlet side does not affect the property of the volatile lubricant

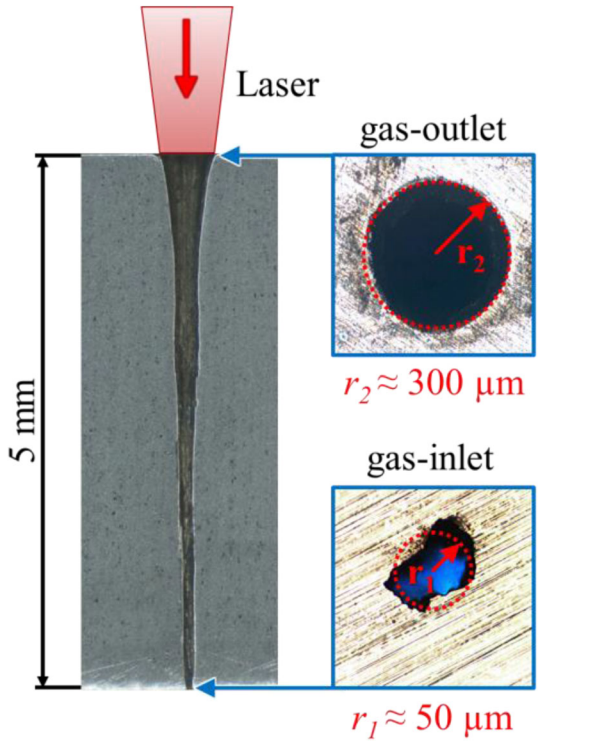

Fig. 5. Cross-section of a microhole in hardened tool steel (1.2379), etched with an Adler solution for 30 s (left). In addition, the gas-outlet (top) and gas-inlet (bottom) cross-sections are shown on the right-hand side. The dotted circles represent equivalent cross-sectional areas where the radius was approximately r_2 = 300 μm and r_1 = 50 μm, respectively.

at the outlet side. About 2.1×10^5 pulses were necessary for the production of this microhole.

CHARACTERIZATION OF THE NEW TRIBOLOGIC SYSTEM

To prove the feasibility of the new tribologic system, various parameter studies were carried out for characterizing its friction behavior. These studies included on the one hand flat strip drawing investigations, referring to the friction conditions in the contact zones of the flange-blank holder and flange-die, and on the other hand stretch-bending tests (SBTs) with different tool radii to characterize the friction behavior at heavily loaded tool radii.

Strip Drawing Investigations

For the strip drawing tests, an existing testing rig was modified as shown in Fig. 6 to ensure the supply of the volatile lubricants. Thereby, the strip drawing jaws have been further developed in three steps to improve the quality of the results. In particular, this further development considered the avoidance of tipping of the jaws, improved contact behavior and high rigidity against elastic deformation due to internal gas pressure as shown in Fig. 6. With the third step of development, all these aspects have been significantly improved.

First investigations on the friction conditions of the new tribologic system using this modified testing rig concentrated on the influence of numbers and arrangements of the microholes.[10] In a further step, different surface structures applied to the jaws were investigated.[11] However, during these strip drawing tests it became clear that the drawing jaws without structured surfaces show the lowest friction coefficients. Therefore, the approach of structured surfaces was not continued.

The influence of various parameters on the coefficient of friction was determined by strip drawing tests with unstructured drawing jaws made of 1.2379 cold work steel and sheet metal samples made of DC05 + ZE. The influence of the number of microholes, microhole diameter, microhole geometry, normal contact pressure and type of lubricating gas was determined. In total, strip drawing tests with 64 parameter combinations and at least 3 repetitions each were carried out.[12]

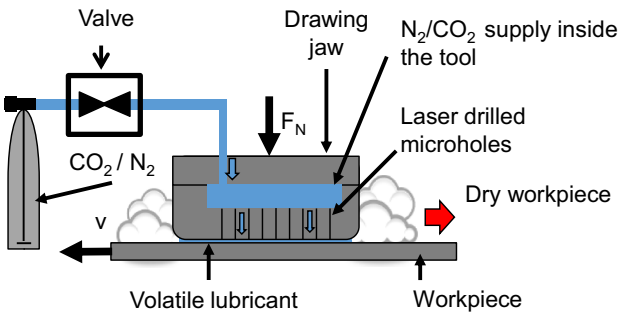

Fig. 6. Setup of the flat strip drawing testing rig.

Obtained results show that regardless of the use of CO_2 and N_2, an arrangement of nine diffusor-shaped microholes in a 3×3 pattern, spanning a rectangle of 5×10 mm, leads to the lowest coefficients of friction. At high normal contact pressures, a smaller gas-inlet diameter of 200 μm leads to lower coefficients of friction. Higher normal contact pressures are more critical; therefore, a gas-inlet diameter of 200 μm was chosen for further investigations.

Stretch-Bending Tests (SBT)

Tool radii of deep drawing tools are the highest loaded areas regarding normal contact pressure. Therefore, radii are very interesting for friction investigations to determine the limits of tribosystems. In this respect, stretch-bending tests (SBTs) were conducted to characterize the friction conditions at tool radii under various main influencing parameters. The setup of the stretch-bending-testing rig used is shown in Fig. 7. Here, the radius inserts contain the previously described integrated laser-drilled microholes. The surfaces of the radius inserts have been polished. The surface roughness of a radius insert with radius R = 12.5 mm, as well as a sheet metal specimen (DC05 + ZE) with a thickness of 0.7 mm was measured. A maximum height value of S_z = 12.8 μm and an arithmetic mean height of S_a = 0.819 μm were measured for the radius insert. The roughness values of the sheet metal specimen were S_z = 23.1 μm and S_a = 1.57 μm. The varied parameters for this test were the retention force (3.4–7 kN), injection angle of lubrication media (30°–60°), type of volatile media ($CO_{2,\ liquid}$ and $N_{2,\ gaseous}$), radius size (R5–R12.5) and arrangement of microholes (single and double line arrangement).

To determine the coefficient of friction via the stretch-bending tests, the analytic method according to the Euler–Eytelwein formula for rope friction was used. Equation 6 shows the equation to calculate the coefficient of friction. Here, θ is the wrap angle of the sheet metal strip, which is constant $\pi/2$, F_t is the tension force, F_r is the retention force, and μ is the calculated mean value of the coefficient of

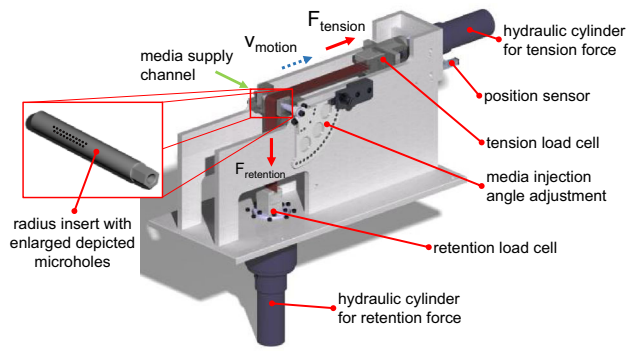

Fig. 7. Setup of the stretch-bending-testing rig using volatile media as lubrication.

friction. Since the sheet metal specimen used was a thin (0.7 mm) soft steel grade, bending effects on SBT results were neglected.

$$\mu = \frac{1}{\theta} \cdot ln\left(\frac{F_t}{F_r}\right), F_t > F_r. \quad (6)$$

The following results are excerpts from the numerous investigations carried out with the SBT rig. All further investigations with single-line arranged microholes and DC05 + ZE sheet material were conducted using an injection angle of 45°, as this angle was found to be optimal in previous studies.[13] All parameter setups were repeated between three and five times.

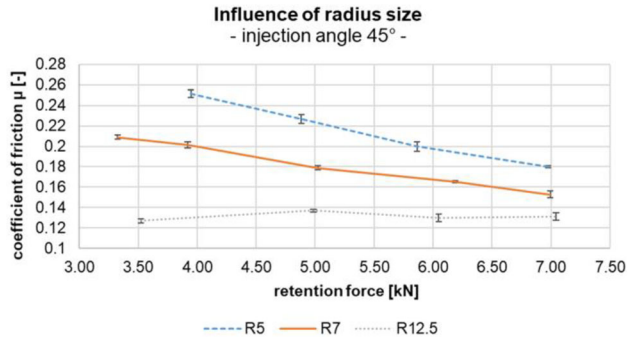

Fig. 8. Influence of radius size on the coefficient of friction, injection angle 45°..

Influence of Radius Size on Coefficient of Friction

The radius size of the drawing edge has a very clear influence on the coefficient of friction, as the coefficient of friction increases with decreasing radius size. This is shown in Fig. 8. This is because smaller radii cause a higher local surface pressure and thus lead to an increased friction coefficient. Furthermore, the diagram shows that in the case of radii R5 and R7.5, the coefficients of friction decrease with increasing retention forces. This can be explained by the improved sealing effect against the free flow of the lubricants due to higher surface pressures. Therefore, the lubricating effect is reduced if the surface pressures are too low. Similar effects can also be observed in conventional tribologic systems.[14]

Comparison of Single- Versus Double-Line Arranged Microholes

In the SBTs with a single-line bore arrangement, several experiments have shown adhesions on the tool radii when using DC05 sheet metal without a zinc coating. These adhesions occurred mainly on the small tool radii, as these cause high contact normal stresses. To address this issue, further tool radius inserts having a double-line microhole arrangement were manufactured, and further investigations on the influence of the double-line microhole arrangement were carried out.

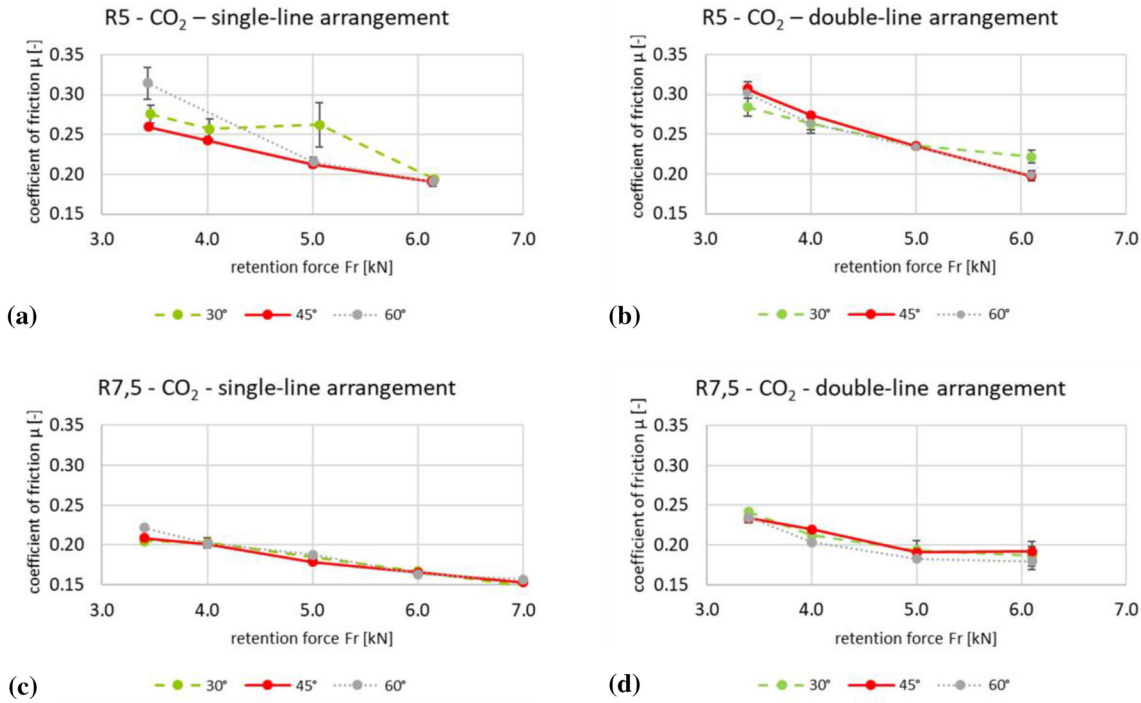

Fig. 9. Results of the stretch-bending-test; (a) and (c) show the results for using a single-line arrangement, while (b) and (d) show the results for double-line arrangement of microholes.

However, as the results in Fig. 9 show, there is no significant difference between the results of the single-line and the double-line microhole arrangement when using CO_2 and the radius R7.5. This is due to the lower surface pressure values compared with the smaller radius R5. By using the small radius, the formation of adhesion at higher retention forces could be completely avoided by introducing the further line of holes. This effect also becomes clear in Fig. 9a and b with the curves for 30° (dashed, R5, single-line versus double-line arrangement). The single-line test results show a further increase in the coefficient of friction at approximately 5 kN, whereas this no longer occurs in the double-line test series. Thus, the associated formation of adhesion was also avoided.

Overall, a significant improvement in terms of adhesion formation and a slight improvement in friction values could be achieved in the SBTs by introducing the double-line bore arrangement. For all parameter setups, the error bars are integrated into the diagrams, but are often too small to be recognized. The reduction of the adhesion formation can be seen because of the strongly reduced error bars depicted in (a) single line arrangement compared with (b) the double-line arrangement of microholes. The results gained for the radius R7.5 mm indicate, however, that the number of injectors achieved with the second line of holes leads to a saturation state of the necessary lubricant quantity supplied. This can be seen from the almost identical coefficients of friction in the single- and double-line radius versions. A further increase in the number of injectors would not lead to any further improvement in the coefficients of friction.

Fig. 10. Drawing die of the rectangular cup tool with free flow out of CO_2 through laser drilled microholes..

FEASIBILITY STUDIES

To prove the feasibility and process stability of the novel tribo-system using volatile lubricants for dry forming, this technology was integrated into a deep-drawing tool for a rectangular cup geometry. For this purpose, > 250 microholes were inserted into the active tool surfaces of the die and blank holder to supply the lubricant by laser drilling. Via the investigations conducted using the real deep-drawing tool, the feasibility and practicability of the novel tribologic system could be proven. Technically, it was possible to implement the media supply into a tool for a rectangular cup (see Fig. 10).

To compare the process stability of the new tribo-system with a conventional tribo-system using mineral oil as the lubricant, working diagrams were determined for each of the tribo-systems. Therefore, the crack and wrinkle limits were determined as a function of the drawing depth for each of the systems by setting different blank holder forces. If the blank holder force was too small, wrinkles of the first type occurred in the component flange. If the blank holder force was too high, the part cracked at the punch radius. Within these limits, good parts could be obtained. The comparison of the working diagrams shown in Fig. 11 reveals a significant improvement in process stability. With both N_2 and

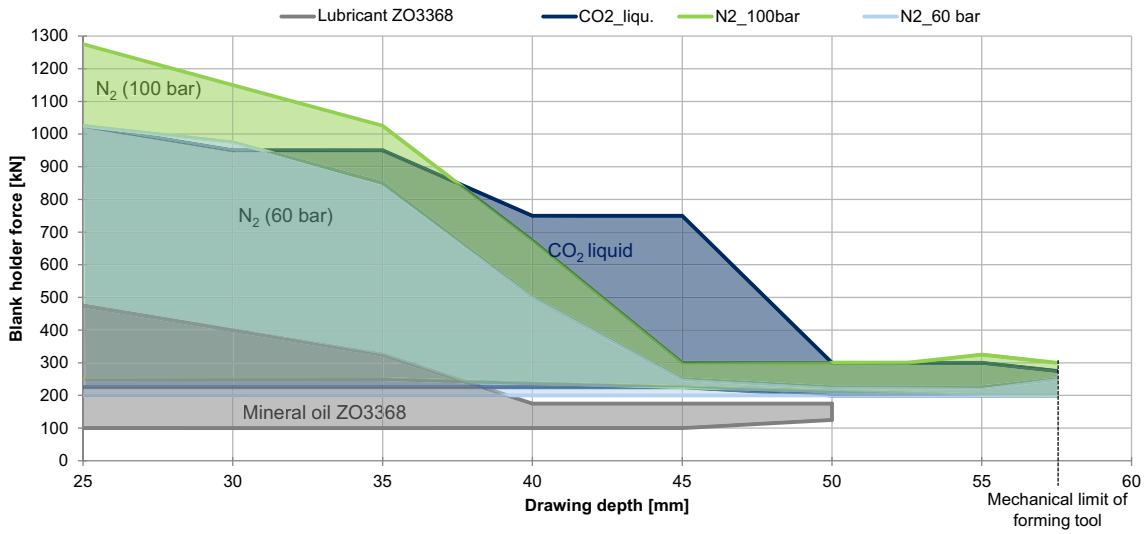

Fig. 11. Working diagrams of the different tribo-systems: mineral oil, N_2 at 60 bar, $CO_{2,\ liquid}$ and N_2 at 100 bar. Adapted from Ref. 15

CO_2, a very high increase in the upper crack limit (up to 250%) can be achieved compared with conventional mineral oil lubrication. Also the maximum achievable drawing depth reaches a much higher value than with mineral oil. The maximum drawing depth could not yet be determined, as the maximum limit of the drawing depth of the tool used was reached at 57.5 mm. Although there was a slight increase in the wrinkle limit, the process stability was increased overall by the significantly rising crack limit when using volatile lubricants.

CONCLUSION AND OUTLOOK

In this article, percussion drilling of particularly deep microholes was described. For this purpose, an equation for the calculation of the required pulse energy needed to achieve the desired drilling depth was shown. High pulse energy of 5 mJ was used to reach the intended drilling depth of 5 mm. Furthermore, the production of the required, longitudinally shaped microholes into the forming tools was described. An analytical model was used for the calculation of the ablation radius at the microhole gas outlet, which showed good agreement with the results of the experiments for a pulse duration of 1 ps. In addition, it could be shown that hardened steel samples with a thickness of 5 mm can be drilled through without creating a heat-affected zone.

Further research will investigate the capability of helical drilling for the optimization of the microhole geometry. In addition, the forming tool that will be used for the endurance tests for the production of deep-drawn rectangular cups will be laser drilled using a custom-built kW-class ultrashort pulsed laser to increase productivity.

Friction studies were conducted to characterize the friction behavior of the novel tribologic system and to prove its feasibility using flat strip drawing investigations and stretch-bending tests (SBTs).

To prove the process stability even under near-series conditions, endurance tests are currently being carried out based on already used rectangular cup and newly developed tool inserts. The aim is to gain knowledge about the wear and suitability of the tribologic system. Here, DC05 + ZE sheet material is also used directly from the coil in the press machine with an integrated cutting operation before the deep-drawing operation. Several test series with 1000 parts each are planned to record running-in behavior and temperature effects that only occur in endurance testing.

The findings obtained in this way will show to what extent the novel tribological system is already suitable for a series application and whether any further optimization is necessary.

ACKNOWLEDGEMENTS

Open Access funding provided by Projekt DEAL. The scientific investigations for this article were funded by the German Research Foundation (DFG) (Grant No. 282210782) within the priority program SPP 1676 Dry Metal Forming-Sustainable Production by Dry Processing in Metal Forming. We thank the German Research Foundation (DFG) for the funding of this research project.

OPEN ACCESS

REFERENCES

1. F. Vollertsen and F. Schmidt, *Int. J. Precis. Eng. Manuf. Green Technol.* 1, 59 (2014).
2. E. Zahedi, C. Woerz, G. Reichardt, G. Umlauf, M. Liewald, J. Barz, R. Weber, D.J. Foerster, and T. Graf, *ICNFT2018 Manuf.* 6, 11 (2019).
3. G. Umlauf, H. Hasselbruch, J. Henze, J. Barz, and A. Mehner, *MATEC Web Conf.* 190, 14012 (2018).
4. D.J. Förster, R. Weber, D. Holder, and T. Graf, *Opt. Express* 26, 11546 (2018).
5. M. Singer, M. Liewald, and A. Feuer, *Key Eng. Mater.* 651, 480 (2015).
6. R. Weber, T. Graf, P. Berger, V. Onuseit, C. Freitag, M. Wiedenmann, and A. Feuer, *Opt. Express* 22, 11312 (2014).
7. D.J. Foerster, R. Weber, and T. Graf, in *Proceedings of the 18th International Symposium on Laser Precision Microfabrication* (2017).
8. D. Breitling, A. Ruf, P. Berger, F. Dausinger, S. Klimentov, P. Pivovarov, T. Kononenko, and V. Konov, in *Proceedings of the SPIE, 5121* (2003).
9. D. Breitling, S. Klimentov, and F. Dausinger, *Top. Appl. Phys.* 96, 75 (2004).
10. M. Liewald, T. Graf, T. Hirth, C. Woerz, S. Boley, E. Zahedi, and G. Umlauf, *Dry Met. Form. OAJ FMT* 1, 22 (2015).
11. G. Umlauf, E. Zahedi, C. Wörz, J. Barz, M. Liewald, T. Graf, and G.E.M. Tovar, *Dry Met. Form. OAJ FMT* 2, 18 (2016).
12. C. Woerz, E. Zahedi, G. Umlauf, M. Liewald, R. Weber, and G.E.M. Tovar, *Dry Met. Form. OAJ FMT* 3, 50–61 (2017).
13. G. Reichardt and M. Liewald, *Proc. Manuf. SheMet* 29, 193 (2019).
14. A. Papaioanu, Einsatz eines neuartigen Verfahrens zum kombinierten Recken und Tiefziehen von Außenhauptbeplankungen aus Feinblech (Beiträge zur Umformtechnik 81, 2016). https://elib.uni-stuttgart.de/bitstream/11682/9127/3/IFU_81_Papaioanu.pdf. Accessed 01 Apr 2020.
15. C. Woerz, G. Reichardt, M. Liewald, E. Zahedi, and R. Weber, *Dry Met. Form. OAJ FMT* 4, 1 (2018).